Model of phytoplankton absorption based on three size classes

Robert J. W. Brewin,[1,2,3,*] Emmanuel Devred,[4,5] Shubha Sathyendranath,[2] Samantha J. Lavender,[1,6] and Nick J. Hardman-Mountford[2,3]

[1]School of Marine Science and Engineering, University of Plymouth, Drake Circus, Plymouth PL4 8AA, UK

[2]Plymouth Marine Laboratory (PML), Prospect Place, The Hoe, Plymouth PL1 3DH, UK

[3]National Centre for Earth Observation, PML, Plymouth PL1 3DH, UK

[4]Department of Oceanography, Dalhousie University, Halifax, Nova Scotia, B3H 4J1, Canada

[5]Ocean Science Division, Bedford Institute of Oceanography, Box 1006, Dartmouth, Nova Scotia, B2Y 4A2, Canada

[6]ARGANS Ltd., Unit 3, Drake Building, Tamar Science Park, Derriford, Plymouth PL6 8BY, UK

*Corresponding author: robr@pml.ac.uk

Received 20 August 2010; revised 3 March 2011; accepted 5 May 2011; posted 23 May 2011 (Doc. ID 133695); published 29 July 2011

Using the phytoplankton size-class model of Brewin *et al.* [Ecol. Model. **221**, 1472 (2010)], the two-population absorption model of Sathyendranath *et al.* [Int. J. Remote. Sens. **22**, 249 (2001)] and Devred *et al.* [J. Geophys. Res. **111**, C03011 (2006)] is extended to three populations of phytoplankton, namely, picophytoplankton, nanophytoplankton, and microphytoplankton. The new model infers total and size-dependent phytoplankton absorption as a function of the total chlorophyll-a concentration. A main characteristic of the model is that all the parameters that describe it have biological or optical interpretation. The three-population model performs better than the two-population model at retrieving total phytoplankton absorption. Accounting for the contributions of picophytoplankton and nanophytoplankton, rather than the combination of both as in the two-population model, improved significantly the retrieval of phytoplankton absorption at low chlorophyll-a concentrations. Class-dependent specific absorption of phytoplankton derived using the model compares well with previously published models. However, the model presented in this paper provides the specific absorption of three size classes and is applicable to a continuum of chlorophyll-a concentrations. Absorption obtained from remotely sensed chlorophyll-a using our model compares well with *in situ* absorption measurements. © 2011 Optical Society of America

OCIS codes: 010.4450, 010.5630, 010.7340, 010.1030, 010.0280.

1. Introduction

We present a phytoplankton absorption model based on size structure [1] and the earlier models of Sathyendranath *et al.* [2] and Devred *et al.* [3]. Understanding the interaction between phytoplankton and the in-water light field is crucial to model ocean primary production and to improve our comprehension of the role of biological processes in the ocean–carbon cycle. The absorption coefficient of phytoplankton (hereafter denoted $a(\lambda)$ where λ is the wavelength) is a fundamental quantity in marine primary production models because (i) it alters the transmission of light underwater [4–8]; (ii) it modifies the photosynthetic response of phytoplankton to available light [9–11]; (iii) it can be used as a direct indicator of phytoplankton abundance [12,13] and phytoplankton size [3,14,15]; and (iv) it can be used as an indicator of environmental variability [13,16].

Several regional and global studies to assess the phytoplankton absorption coefficient have been

0003-6935/11/224535-15$15.00/0

undertaken in the past few decades [7,17–20]. It is well known that the phytoplankton absorption coefficient is a function of the dominant phytoplankton pigment, chlorophyll-a, and that this relationship is directly linked to changes in both pigment composition and size structure [20–25].

Power-law or polynomial expressions have proven useful predictors of the phytoplankton absorption coefficient as a function of the chlorophyll-a concentration [17,18,20,26–28]. Alternatively, models have been proposed based on Michaelis–Menten-type equations [7,19]. However, such approaches have limitations at extreme values of chlorophyll-a concentrations and the interpretation of the model parameters is difficult [3,19].

Recently, total phytoplankton absorption has been expressed as the contribution of two populations of optically distinct phytoplankton [2,3,14]. Such approaches ensure realistic values of the specific absorption coefficient of phytoplankton (absorption per unit chlorophyll-a, $a^*(\lambda)$) when applying the model to extreme values of chlorophyll-a concentration, since the range of values of $a^*(\lambda)$ is bounded by the two values associated with the two populations. Furthermore, the parameters of the model have biological and bio-optical interpretation.

Devred *et al.* [3] extended the Sathyendranath *et al.* [2] model to derive $a^*(\lambda)$ for the two optically distinct phytoplankton populations. Assuming that $a^*(440)$ of large-celled populations of phytoplankton would be smaller than 0.05 (m^2 $[mg\,C]^{-1}$), Devred *et al.* [3] related the large-celled population to microphytoplankton and the small-celled population to combined nano-picophytoplankton that constitute the remaining autotrophic pool.

It is well documented that small phytoplankton have a higher specific absorption coefficient than large phytoplankton [14,22,23,29,30]. Some biogeochemical functions of phytoplankton are also related to cell size. Picophytoplankton have a high surface-to-volume ratio, and, therefore, absorb nutrients with high efficiency under nutrient-limited conditions and sink more slowly than larger cells [31]. Nanophytoplankton are larger than picophytoplankton and some members of the class contribute to the cycling of $CaCO_3$ and dimethylsulphide.

Uitz *et al.* [30] calculated $a^*(\lambda)$ of microphytoplankton, nanophytoplankton, and picophytoplankton by utilizing high performance liquid chromatography (HPLC) analysis. Although a pigment-based classification of phytoplankton does not strictly represent the true size classes of phytoplankton, making it indicative rather than definitive [32,33], pigment composition and cell size are highly correlated, so that, with some caution, the pigment-based classification can be used as a proxy for size class [1,15,20,33,34]. In the Uitz *et al.* [30] model, the proportions of the three size classes in the autotrophic pool are determined according to a small number of class intervals in chlorophyll-a concentrations [33], which may introduce unrealistic spatial discontinuities when satellite data are used to map the distribution of these size classes.

In this paper, using the approach of Brewin *et al.* [1], we extend the two-population absorption model of Sathyendranath *et al.* [2] and Devred *et al.* [3] to three size classes of phytoplankton. As with the model of Uitz *et al.* [30], the three-population model yields the specific absorption coefficients of three size classes (microphytoplankton, nanophytoplankton, and picophytoplankton), and furthermore, it can be applied to a continuum of chlorophyll-a concentrations. The performance of the model, when used to retrieve total phytoplankton absorption for a given chlorophyll-a concentration, is compared with a power-law model and the Devred *et al.* [3] two-component model fitted to the same dataset. Then, the specific absorption coefficients of the three size classes derived using the new model are compared with the results of Ciotti *et al.* [14] and Uitz *et al.* [30] for field data, as well as with results based on laboratory cultures. Finally, absorption coefficient inferred from remotely sensed chlorophyll-a using the model is compared with the corresponding *in situ* data.

2. Methodology

A. *In Situ* Data

The NASA bio-Optical Marine Algorithm Dataset (NOMAD) was used for model development and intercomparison [35]. NOMAD is a global, high-quality, *in situ*, bio-optical dataset, publicly available for algorithm development and ocean-color satellite validation (samples located within either the first optical depth or at a depth <10 m). A subset of NOMAD made of colocated $a(\lambda)$ (20 wavelengths between 405 and 683 nm) and pigment concentration derived from HPLC, was downloaded from the NASA website (Version 1.3.h, 22/02/2007 HPLC evaluation dataset). This consisted of 265 measurements collected in various oceans insuring high variability in the dataset. The pigment and $a(\lambda)$ dataset was quality controlled according to Aiken *et al.* [36], reducing the number of measurements to 256, and is hereafter referred to as database A.

The model was used to estimate phytoplankton absorption as a function of chlorophyll-a, estimated from remote-sensing reflectances using an empirical model [37], and the results were compared with *in situ* data from the NASA NOMAD dataset (Version 2.0 w APLHA, 18/07/2008, OOXIX IOP Algorithm Workshop evaluation dataset [35,38]) from which data points that were common to database A were eliminated, such that the comparison might be regarded as an independent test of the performance of the model in a remote-sensing context. The resulting dataset consisted of 634 matched remote-sensing reflectances at SeaWiFS visible wavelengths, *in situ* absorption coefficient of phytoplankton, $a(\lambda)$, and chlorophyll-a concentration. This validation dataset is hereafter referred to as database B.

B. Data Analysis

Diagnostic pigments [32] were used to compute the size-specific chlorophyll-a concentrations and the fractions of a given size class in the total chlorophyll-a concentration for each sample in database A. First, we note that, according to Uitz *et al.* [33], the chlorophyll-a concentration can be derived from the seven diagnostic pigments, such that

$$C_w = \sum_{i=1}^{7} W_i P_i, \tag{1}$$

where C_w = total chlorophyll-a concentration calculated from the sum of the pigments, $[\mathbf{W}] = \{1.41; 1.41; 1.27; 0.35; 0.6; 1.01; 0.86\}$ and $[\mathbf{P}] = \{$fucoxanthin; peridinin; 19′-hexanoyloxyfucoxanthin; 19′-butanoyloxyfucoxanthin; alloxanthin; chlorophyll-b and divinyl chlorophyll-b; zeaxanthin$\}$. According to Uitz *et al.* [33], as modified by Brewin *et al.* [1] to account for picoeukaroytes in ultra-oligotrophic environments, the fractions $[\mathbf{F}]$ of the chlorophyll-a concentration (C) associated with each size class can be inferred as

$$F_p = \begin{cases} \frac{(-12.5C+1)W_3P_3}{C_w} + \frac{\sum_{i=6}^{7} W_i P_i}{C_w} & \text{if } C < 0.08\ \text{mg m}^{-3} \\ \frac{\sum_{i=6}^{7} W_i P_i}{C_w} & \text{if } C > 0.08\ \text{mg m}^{-3}, \end{cases} \tag{2}$$

$$F_n = \begin{cases} \frac{12.5CW_3P_3}{C_w} + \frac{\sum_{i=4}^{5} W_i P_i}{C_w} & \text{if } C < 0.08\ \text{mg m}^{-3} \\ \frac{\sum_{i=3}^{5} W_i P_i}{C_w} & \text{if } C > 0.08\ \text{mg m}^{-3}, \end{cases} \tag{3}$$

$$F_m = \frac{\sum_{i=1}^{2} W_i P_i}{C_w}. \tag{4}$$

In this paper, subscripts p, n, and m refer to picophytoplankton, nanophytoplankton, and microphytoplankton, respectively, and the picophytoplankton and nanophytoplankton fractions when combined into a single fraction, is referred to as $F_{p,n} = F_p + F_n$. The fractions of each size class can then be applied to the *in situ* chlorophyll-a concentrations (C) to derive the size-specific chlorophyll-a concentrations for each sample in database A:

$$C_p = F_p C, \tag{5}$$

$$C_n = F_n C, \tag{6}$$

$$C_{p,n} = F_{p,n} C, \tag{7}$$

$$C_m = F_m C. \tag{8}$$

C. Model Development

In this section, using the model of Brewin *et al.* [1], we extend the two-population absorption model of Sathyendranath *et al.* [2] and Devred *et al.* [3] to a three-population absorption model of phytoplankton size class. To simplify the notation in our manuscript we have used $a(\lambda)$ to represent phytoplankton absorption, though it is commonly used for total absorption. Appendix A provides a key to notations used in the paper. The phytoplankton absorption coefficient can be expressed as

$$a(\lambda) = a^*(\lambda) C. \tag{9}$$

Here we assume the total chlorophyll-a concentration (C) is the sum of chlorophyll-a concentrations in the picophytoplankton (C_p), nanophytoplankton (C_n), and microphytoplankton (C_m) components, such that

$$C = \sum_{i=1}^{3} C_i, \tag{10}$$

where $i = \{$picophytoplankton, nanophytoplankton and microphytoplankton$\}$. Sathyendranath *et al.* [2] gave an expression for the chlorophyll-a concentration of small cells as a function of the total chlorophyll-a concentration. If we treat small cells as being the combination of picophytoplankton and nanophytoplankton [1], then their combined chlorophyll-a concentration ($C_{p,n}$) can be expressed as

$$C_{p,n} = C^m_{p,n}[1 - \exp(-S_{p,n} C)], \tag{11}$$

where $C^m_{p,n}$ is the asymptotic maximum value for $C_{p,n}$, and $S_{p,n}$ determines the initial slope of the curve. It follows that

$$C_m = C - C_{p,n}. \tag{12}$$

Furthermore, according to Brewin *et al.* [1], the model of Sathyendranath *et al.* [2] can also be used to calculate the picophytoplankton chlorophyll-a concentration (C_p) from total chlorophyll-a (C), such that

$$C_p = C^m_p[1 - \exp(-S_p C)], \tag{13}$$

where C^m_p is the asymptotic maximum value for C_p and S_p determines the initial slope of the curve. Therefore, C_n can be calculated according to

$$C_n = C_{p,n} - C_p. \tag{14}$$

The fractions of each size class (F_p, F_n, and F_m) can then be derived from

$$F_p = \frac{C^m_p[1 - \exp(-S_p C)]}{C}, \tag{15}$$

$$F_n = \frac{C^m_{p,n}[1 - \exp(-S_{p,n} C)] - C^m_p[1 - \exp(-S_p C)]}{C}, \tag{16}$$

$$F_{p,n} = \frac{C^m_{p,n}[1 - \exp(-S_{p,n} C)]}{C}, \tag{17}$$

$$F_m = \frac{C - C^m_{p,n}[1 - \exp(-S_{p,n}C)]}{C}. \quad (18)$$

The unknown parameters C^m_p, $C^m_{p,n}$, S_p, and $S_{p,n}$ were obtained by performing a nonlinear least squares regression (Levenberg–Marquardt [39], IDL Routine MPFITFUN) of F_p and $F_{p,n}$ on C from database A using Eqs. (15) and (17). The retrieved parameters are given in Table 1. Here we assume the total phytoplankton absorption coefficient ($a(\lambda)$) is the sum of the picophytoplankton ($a_p(\lambda)$), nanophytoplankton ($a_n(\lambda)$), and microphytoplankton ($a_m(\lambda)$) contributions such that

$$a(\lambda) = \sum_{i=1}^{3} a^*_i(\lambda) C_i, \quad (19)$$

where $i = \{\text{picophytoplankton, nanophytoplankton and microphytoplankton}\}$. Expanding Eq. (19) by inserting Eqs. (11)–(14) yields the expression

$$\begin{aligned} a(\lambda) = {} & a^*_p(\lambda) C^m_p [1 - \exp(S_p C)] \\ & + a^*_n(\lambda)\{C^m_{p,m}[1 - \exp(-S_{p,n}C)] \\ & - C^m_p [1 - \exp(-S_p C)]\} \\ & + a^*_m(\lambda)\{C - C^m_{p,n}[1 - \exp(-S_{p,n}C)]\}. \end{aligned} \quad (20)$$

Having retrieved C^m_p, $C^m_{p,n}$, S_p and $S_{p,n}$, Eq. (20) was then fitted to C and $a(\lambda)$ from database A to derive $a^*_p(\lambda)$, $a^*_n(\lambda)$, and $a^*_m(\lambda)$ at each of the 20 wavelengths shown in Table 2. To examine whether the retrieved specific absorption coefficients are realistic, they are compared with laboratory measurements [22,23,40,41], *in situ* measurements [42], and size-specific absorption coefficients retrieved using other approaches [3,14,30,43].

Table 1. Parameter Values Derived from Fitting Eqs. (15), (17), and (23) to Database A

	$C^m_{p,n}$ [mg m^{-3}]	$S_{p,n}$	C^m_p [mg m^{-3}]	S_p
Three-population model [Eq. (20)]	0.775	1.152	0.146	5.118
Two-population model [3]	0.929	1.077	-	-

The performance of our model (as well as of other models tested later) was quantified using the root mean square error (RMSE) between the retrieved and measured absorption coefficients. The RMSE were computed in relative values so as to give equal weight to all measurements and expressed in percentages according to

$$\text{RMSE}\% = \left[\frac{1}{N}\sum_{i=1}^{N}\left(\frac{a_{i,E}(\lambda) - a_{i,M}(\lambda)}{a_{i,M}(\lambda)}\right)^2\right]^{1/2} 100, \quad (21)$$

where N is the number of samples. The subscript E denotes the estimated variable, and the subscript M denotes the measured variable. The RMSE% values as well as the Pearson correlation coefficients (r) between the model estimates and corresponding observations in database A are given in Table 2.

D. Comparison with Other Phytoplankton Absorption Models

1. *Models That Relate Phytoplankton Absorption Coefficients to the Chlorophyll-a Concentration*

The absorption model developed in the previous section was compared with a variety of existing

Table 2. Size-specific Absorption Coefficients (m^2 [mg C]$^{-1}$) Retrieved from Database A Using the Three-Population Model [Eq. (20)], the Devred *et al.* [3] Model [Eq. (23)], As Well As Parameters for the Power-Law Model [Eq. (22)]

	Three-Population Model [Eq. (20)]					Two-Population Model [3]				Power-Law Model			
λ (nm)	a^*_p	a^*_n	a^*_m	RMSE%	r	$a^*_{p,n}$	a^*_m	RMSE%	r	A	B	RMSE%	r
405	0.1053	0.0176	0.0167	50.9	0.871	0.0499	0.0149	62.6	0.881	0.0317	0.3241	52.5	0.883
411	0.1147	0.0256	0.0169	46.2	0.879	0.0555	0.0163	55.4	0.885	0.0358	0.3427	46.4	0.887
443	0.1552	0.0333	0.0225	38.5	0.906	0.0708	0.0206	45.5	0.911	0.0477	0.3485	38.4	0.911
455	0.1484	0.0280	0.0203	37.8	0.910	0.0648	0.0182	45.0	0.915	0.0437	0.3604	37.7	0.915
465	0.1318	0.0347	0.0182	36.8	0.912	0.0632	0.0167	42.8	0.917	0.0419	0.3580	36.0	0.916
489	0.1031	0.0238	0.0143	36.8	0.909	0.0480	0.0125	43.0	0.915	0.0318	0.3556	36.5	0.915
510	0.0611	0.0125	0.0109	38.5	0.920	0.0281	0.0104	45.2	0.923	0.0198	0.2994	39.0	0.922
520	0.0417	0.0103	0.0093	39.0	0.928	0.0207	0.0091	44.8	0.929	0.0151	0.2509	39.6	0.928
530	0.0285	0.0083	0.0081	41.4	0.930	0.0157	0.0082	46.3	0.930	0.0117	0.1960	41.8	0.929
550	0.0170	0.0036	0.0057	54.4	0.917	0.0094	0.0059	61.7	0.917	0.0070	0.1426	54.2	0.916
555	0.0155	0.0024	0.0049	60.0	0.912	0.0081	0.0052	70.0	0.912	0.0059	0.1453	60.0	0.911
560	0.0136	0.0017	0.0043	81.5	0.909	0.0070	0.0045	89.2	0.909	0.0050	0.1372	75.5	0.907
565	0.0131	0.0007	0.0038	73.5	0.906	0.0063	0.0041	93.7	0.906	0.0044	0.1459	74.8	0.904
570	0.0122	0.0005	0.0037	77.9	0.908	0.0058	0.0040	99.8	0.909	0.0041	0.1314	78.9	0.907
590	0.0095	0.0038	0.0041	104	0.927	0.0068	0.0042	108	0.927	0.0048	0.0946	92.7	0.927
619	0.0114	0.0044	0.0052	54.9	0.943	0.0074	0.0055	55.2	0.943	0.0060	0.0924	52.0	0.942
625	0.0130	0.0046	0.0056	44.5	0.945	0.0079	0.0058	45.8	0.945	0.0066	0.1040	43.3	0.944
665	0.0284	0.0137	0.0137	33.6	0.956	0.0195	0.0139	35.6	0.957	0.0163	0.0990	33.6	0.957
670	0.0348	0.0199	0.0165	31.2	0.958	0.0254	0.0168	33.0	0.958	0.0208	0.1147	31.1	0.958
683	0.0264	0.0207	0.0121	31.4	0.957	0.0225	0.0125	32.8	0.958	0.0174	0.1428	31.5	0.958

Root mean square error percentages (RMSE%) and linear Pearson correlation coefficients (r) are provided for each model.

phytoplankton absorption models. Power-law expressions have proven useful descriptors of the phytoplankton absorption coefficient as a function of the chlorophyll-a concentration [17,20,26–28,44]. The power-law model can be expressed as

$$a(\lambda) = A(\lambda)C^{(1-B(\lambda))}, \tag{22}$$

where $A(\lambda)$ and $B(\lambda)$ are positive, wavelength-dependent parameters (of the same formulation as in Table 2 of Bricaud *et al.* [27]). Equation (22) was fitted to $a(\lambda)$ as a function of C from database A to derive the parameters of A and B (shown in Table 2 together with correlation coefficients (r) and RMSE%).

The Sathyendranath *et al.* [2] model is expressed as

$$a(\lambda) = C_{p,n}^{m}[a_{p,n}^{*}(\lambda) - a_{m}^{*}(\lambda)][1 - \exp(-S_{p,n}C)] + a_{m}^{*}(\lambda)C. \tag{23}$$

Their model was not based on pigment composition. Instead, it was designed to classify the phytoplankton population into two optically distinct classes. Nevertheless, Devred *et al.* [3] showed, using data from a variety of ecosystems, that when $a_{m}^{*}(440) < 0.05$ (m^2 [mg C]$^{-1}$), the corresponding population was well correlated with the microphytoplankton fraction estimated independently by HPLC pigment analysis. Conversely, the population with the higher specific absorption coefficient corresponded to the combined nanophytoplankton and picophytoplankton. Therefore, when dealing with the Sathyendranath *et al.* [2] model, we assume that the model parameters $C_{p,n}^{m}$ and $S_{p,n}$ in Eqs. (20) and (23) may be treated analogous to each other, despite differences in the method by which they are determined. Whereas in the model presented here, HPLC data are used to determine the parameters, in the Sathyendranath *et al.* [2] model, Eq. (23) is fitted directly to absorption and chlorophyll data to retrieve model parameters.

Equation (23) was fitted to $a(\lambda)$ as a function of C to samples in database A following the procedure described in Section 2.D of Devred *et al.* [3]. First, the Sathyendranath *et al.* [2] model was fitted to the wavelengths from 411 to 489 nm to derive $U(\lambda)$, $S_{p,n}$, and $a_{m}^{*}(\lambda)$, where $U(\lambda)$ refers to the composite parameter $C_{p,n}^{m}[a_{p,n}^{*}(\lambda) - a_{m}^{*}(\lambda)]$. The computed $S_{p,n}$ values were then averaged and used to compute $U(\lambda)$ and $a_{m}^{*}(\lambda)$ over the entire spectral range. The parameters $C_{p,n}^{m}$ and $a_{p,n}^{*}(\lambda)$ were then computed using Eqs. (5) and (10) in Devred *et al.* [3]. This procedure assumes that as C tends to zero C_m (the chlorophyll concentration associated with microphytoplankton) tends to zero and as a consequence $S_{p,n}$ $C_{p,n}^{m}$ tends to 1. The computed parameters are given in Tables 1 and 2 together with r and RMSE% values. Note that the retrieved $a_{m}^{*}(443)$ value is less than 0.05 (m^2 [mg C]$^{-1}$) and, therefore, according to Devred *et al.* [3], we can assume the small-celled population is combined pico-nanophytoplankton and the large-celled population microphytoplankton.

2. *Models That Derive Size-Class-Dependent Specific Phytoplankton Absorption*

The Ciotti *et al.* [14] model is expressed in terms of $a^{*}(\lambda)$:

$$a^{*}(\lambda) = G_p a_{p}^{*}(\lambda) + (1 - G_p)a_{m}^{*}(\lambda), \tag{24}$$

where $a_{p}^{*}(\lambda)$ and $a_{m}^{*}(\lambda)$ represent the specific absorption coefficients of picophytoplankton and microphytoplankton, respectively (Table 3 of Ciotti *et al.* [14]), and G_p represents the fractional contribution of picophytoplankton to the total absorption coefficient, accounting for both pigment composition and cell size. Note that G_p in Eq. (24) is represented as $S_{\langle f \rangle}$ in Ciotti *et al.* [14] and their notation has been changed here to avoid confusion with parameters $S_{p,n}$ and S_p used in this study. In deriving G_p, Ciotti *et al.* [14] physically separated phytoplankton samples into size classes using filtration and determined the absorption spectra associated with each size class. The specific absorption coefficients derived by Ciotti *et al.* [14] (see their Table 3), and the updated picophytoplankton specific absorption coefficients of Ciotti and Bricaud [43] (see their Web Appendix 1), were used for comparison with the specific absorption coefficients derived using the model presented here [Eq. (20)].

The Uitz *et al.* [30] model is expressed as

$$a^{*}(\lambda) = \frac{1}{C}\sum_{i=1}^{3} C_i a_{i}^{*}(\lambda) \exp\left(-R_i \frac{z}{Z_p}\right), \tag{25}$$

where $i = \{\text{picophytoplankton, nanophytoplankton and microphytoplankton}\}$ and R_i represent the slopes describing the variations in $a_{i}^{*}(\lambda)$ along the vertical z/Z_p axis (z = depth and Z_p = euphotic depth). Note that R_i has the notations S_{micro}, S_{nano}, and S_{pico} in Uitz *et al.* [30] for the different size classes and their notation has been changed here to avoid confusion with the parameters $S_{p,n}$ and S_p in the model presented here. Because the study is limited to the surface layer of the ocean, z/Z_p was set to zero and, therefore, Eq. (25) reduces to

$$a^{*}(\lambda) = \frac{1}{C}\sum_{i=1}^{3} C_i a_{i}^{*}(\lambda). \tag{26}$$

The parameters of Eq. (26) are given in Uitz *et al.* [30] Web Appendix 1 and were used for comparison with the specific absorption coefficients derived using the model presented here [Eq. (20)].

3. Results and Discussion

A. Three-Population Absorption Model

To examine how well the three-population model fits the pigment observations from database A the model is plotted against the observations in Fig. 1. It can be seen that the model captures the general trend in both the size-specific chlorophyll-a concentrations [Figs. 1(a)–1(d)] and the fractional contributions [Figs. 1(e)–1(h)]. The retrieved coefficients $a_p^*(\lambda)$, $a_n^*(\lambda)$, and $a_m^*(\lambda)$ derived by fitting the three-population model to database A are plotted in Fig. 2(a), and the same spectra are shown in Fig. 2(b) after normalization at 443 nm to highlight differences in their spectral form. The specific absorption coefficients of all the three size classes have typical peaks around 443 and 670 nm associated with chlorophyll-a absorption.

Microphytoplankton exhibit low $a^*(\lambda)$ at all wavelengths (Table 2), and the flattest spectral shape [Fig. 2(b)], which is consistent with previous studies [3,30,45–47] and can be linked to the strong package effect occurring in large-celled phytoplankton [20,22,23].

The nanophytoplankton absorption spectrum ($a_n^*(\lambda)$) is higher than $a_m^*(\lambda)$ but lower than $a_p^*(\lambda)$ at most wavelengths (Table 2). In agreement with previous studies [30], the nanophytoplankton spectrum exhibits a distinct peak at 465 nm characteristic of the pigments 19′-hexanoyloxyfucoxanthin and 19′-butanoyloxyfucoxanthin [48]. However, this spectral feature is accentuated when compared with other nanophytoplankton spectra [22,30] and further investigation is needed to verify if it is realistic.

Picophytoplankton consistently display the highest specific absorption consistent with their small size. This is enhanced in the blue wavelengths, probably due to the presence of nonphotosynthetic carotenoids, such as zeaxanthin or β-carotene, that absorb in this region of the spectrum. The picophytoplankton spectrum also exhibits a small peak at 490 nm, which may be attributed to the photoprotective pigment zeaxanthin [49].

The size-specific $a^*(443)$ values retrieved from the model are consistent with previous laboratory studies on microphytoplankton [23,41] and nanophytoplankton [22]. For picophytoplankton, the specific absorption coefficient at 443 nm ($a_p^*(443)$) obtained ($0.15\,\mathrm{m}^2\ [\mathrm{mg}\,C]^{-1}$) is lower than that derived from some laboratory monospecific cultures of

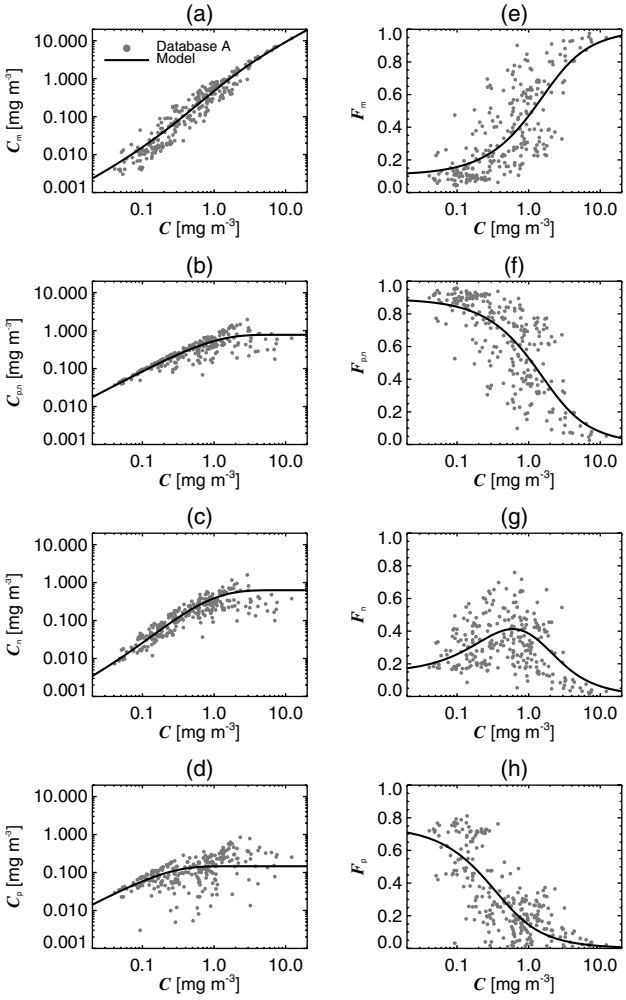

Fig. 1. Three-population model fitted to pigment data from database A, (a)–(d) show the model plotted against the size-specific chlorophyll-a concentrations and (e)–(h) show the model plotted against the size-specific fractional contributions to the total chlorophyll-a concentration.

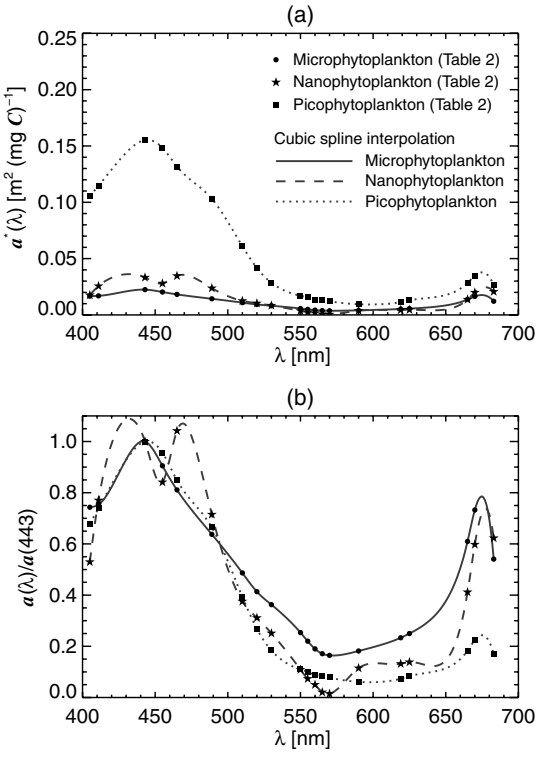

Fig. 2. Specific absorption curves retrieved from database A using the three-population absorption model: (a) magnitude and (b) shape normalized at 443 nm.

Prochlorococcus (e.g., 0.19 m^2 [mg C]$^{-1}$ [40]), although consistent with other laboratory studies on picophytoplankton (e.g., 0.14–0.16 m^2 [mg C]$^{-1}$ [50,51]). Turning to field studies, $a_p^*(443)$ obtained for picophytoplankton in this study is consistent with that observed *in situ* by Babin *et al.* [42] at the surface in a picophytoplankton-dominated site in the North Atlantic (0.16 m^2 [mg C]$^{-1}$).

Figure 3(a) shows the absorption spectrum of phytoplankton for chlorophyll-a concentration (C) ranging from 0.01 to 5 mg m^{-3}, and Figs. 3(b)–3(d) show the fractional contributions to the absorption coefficient from the three size classes at the different wavelengths. The picophytoplankton contribution is the highest when the total phytoplankton absorption coefficient is low (e.g. 0.00 to 0.03 m^{-1} at 443 nm); as the total phytoplankton absorption coefficient increases (e.g., 0.03 to 0.07 m^{-1} at 443 nm), the nanophytoplankton contribution becomes higher; and as the total phytoplankton absorption coefficient increases beyond 0.07 m^{-1} at 443 nm, the microphytoplankton contribution becomes dominant. Superimposed on the first-order relationship associated with concentrations are the spectral characteristics of each size class shown in Fig. 2. When the nanophytoplankton and picophytoplankton fractions are high, their effects on the shape of the total absorption spectra become pronounced [Figs. 3(b) and 3(c)]. When total absorption is high, the microphytoplankton contribution is more pronounced in the green and red portions of the absorption spectrum as a consequence of the relatively flat shape of its absorption spectrum [Fig. 3(d)]. By decomposing the total phytoplankton absorption spectra we begin to understand how it is spectrally influenced by varying phytoplankton composition.

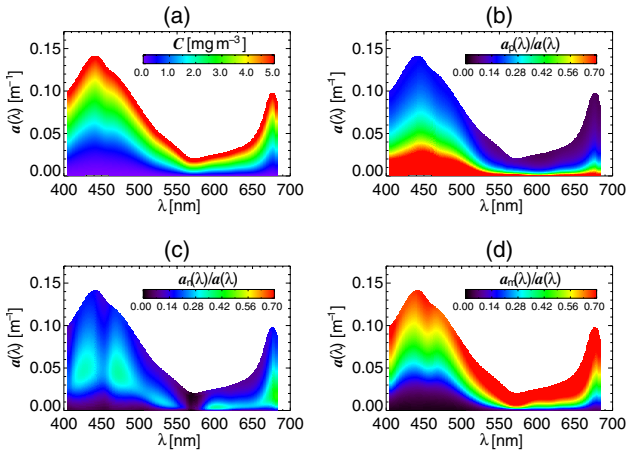

Fig. 3. (Color online) (a) Phytoplankton absorption coefficient reconstructed from the chlorophyll-a concentration according to the three-population absorption model, (b)–(d) show the fractional contribution from the picophytoplankton, nanophytoplankton, and microphytoplankton size classes, respectively (cubic spline used to interpolate between wavelengths in Table 2).

B. Comparison with Other Approaches

1. *Phytoplankton Absorption Coefficients as a Function of the Chlorophyll-a Concentration*

The Power-Law Model

Figures 4(a)–4(c) shows *in situ* absorption of phytoplankton from database A versus chlorophyll-a at 443, 555, and 670 nm, on which the three-population model and the power-law model fitted to the same database (Table 2) are superimposed. Figure 4(d) shows the RMSE% (given in Table 2) as a function of wavelength for the two models. In comparison with the power-law model, the three-population absorption model yielded statistically similar RMSE% across the 20 wavelengths (t-test, $p = 0.88$). The r values in Table 2 are generally comparable between the two approaches (>0.87), and statistically similar across the 20 wavelengths (t-test, $p = 0.81$). When using a power-law model with the coefficients of Bricaud *et al.* [20] at 440 nm, the three-population model yielded lower RMSE% at 443 nm (38.5% in comparison with 60.9%, Fig. 4(d)].

At low chlorophyll-a concentrations in the blue region [Fig. 4(a)], the power-law model predicts higher $a(\lambda)$ values than the three-population model. To investigate this further we plotted the specific absorption coefficient ($a^*(\lambda)$) as a function of the chlorophyll-a concentration according to both the three-population absorption model [Fig. 5(a)] and the power-law model [Fig. 5(b)] using parameters in Tables 1 and 2. We also computed the mean dominant specific absorption coefficients for

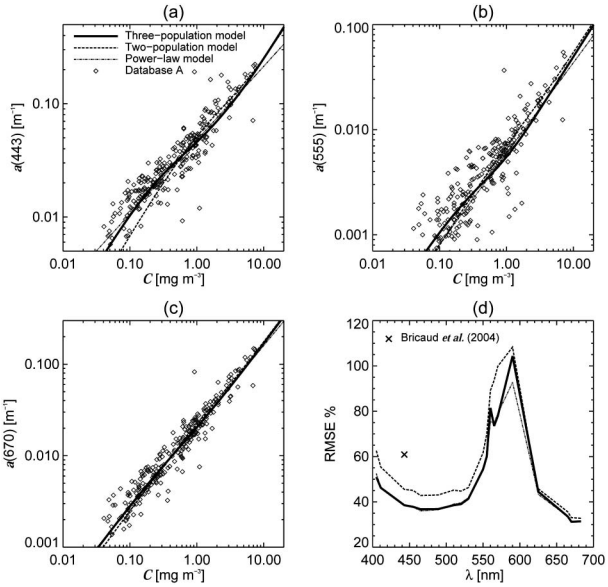

Fig. 4. The three-population model, the two-population model [3], and the power-law model plotted against database A, with which they were parameterized, for the wavelengths (a) 443 nm, (b) 555 nm, and (c) 670 nm. Figure 4(d) shows the root mean squared error percentages from Table 2 as a function of wavelength for the three models.

microphytoplankton, nanophytoplankton, and picophytoplankton in database A using only those samples in database A for which F_p, F_n, or F_m were >0.65. The specific absorption coefficients for each size class was then averaged and are superimposed in Fig. 5 together with their confidence levels.

Whereas the three-population model represents the variability in the specific absorption coefficient between the three size classes, the power-law model overestimates the specific absorption coefficient in the blue-green region (400–550 nm) when extrapolating to lower chlorophyll-a concentrations than the minimum value in database A. Lutz *et al.* [19] and Devred *et al.* [3] have highlighted that a model based on the power-law can fail at extremely low chlorophyll-a concentrations as the specific absorption coefficient tends to infinity. The three-population model adopted from Sathyendranath *et al.* [2] and Devred *et al.* [3] constrains the specific absorption coefficients to realistic values based on phytoplankton size structure, and the parameters of the model offer direct optical and biological interpretation.

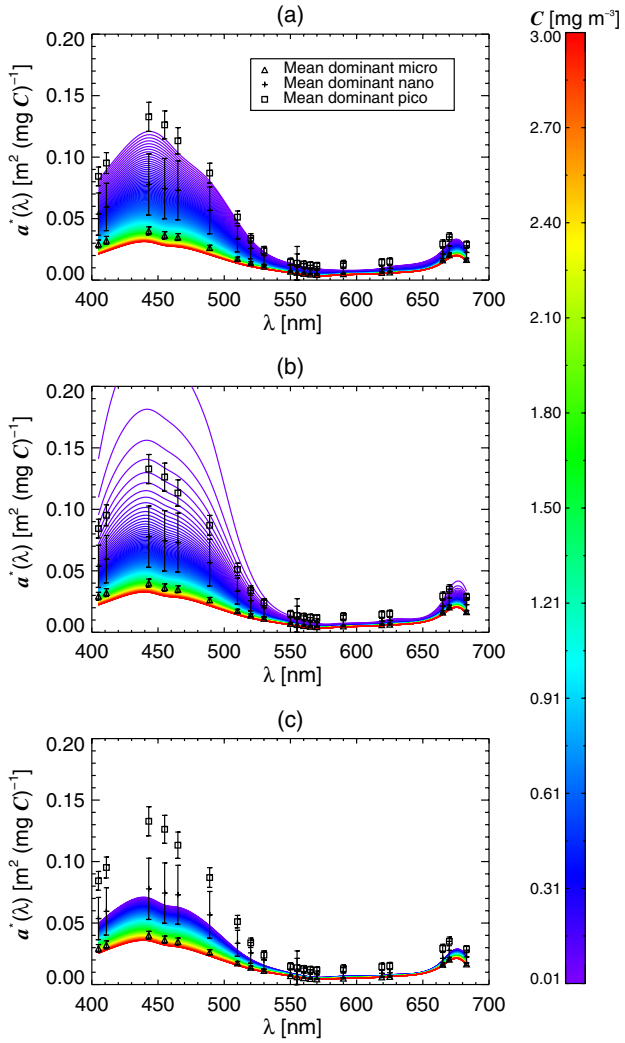

Fig. 5. (Color online) (a) $a^*(\lambda)$ calculated from the three-population model for a range of chlorophyll-a concentrations, (b) $a^*(\lambda)$ calculated from the power-law model for a range of chlorophyll-a concentrations, and (c) $a^*(\lambda)$ calculated from the two-population model [3] for a range of chlorophyll-a concentrations. All models were fitted to database A, with parameters given in Tables 1 and 2 and a cubic spline used to interpolate between wavelengths in Table 2. Superimposed are the mean dominant size-specific $a^*(\lambda)$ spectra from database A and their 95% confidence levels.

The Model of Devred et al. [3]

The specific absorption coefficients calculated using the three-population model and the two-population model (Devred *et al.* [3], with the model parameters fitted to the database A) given in Table 2, and the specific absorption coefficients calculated in the Devred *et al.* [3] study for global applications are plotted in Fig. 6(a). At all wavelengths $a^*_{p,n}(\lambda)$ calculated using the two-population model lies between the $a^*_p(\lambda)$ and $a^*_n(\lambda)$ spectra calculated using the three-population model, as expected.

The $a^*_m(\lambda)$ derived from the database A using the two-population model are slightly higher at most wavelengths when compared with the spectra derived from the global dataset used in the Devred *et al.* [3] study. The global dataset used in Devred *et al.* [3] ranged in chlorophyll-a concentrations between 0.05 to 28.0 mg m^{-3}, whereas the values in database A ranged between 0.04 and 12.2 mg m^{-3}. It might be expected that the higher chlorophyll-a concentrations in the Devred *et al.* [3] study would yield lower $a^*_m(\lambda)$ values as larger phytoplankton cells are sampled at these very high chlorophyll-a concentrations. The differences could also be indicative of regional or temporal variations in the phytoplankton composition.

The microphytoplankton specific absorption coefficients, $a^*_m(\lambda)$, calculated using the three-population model are slightly higher than for the two-population model using database A in the blue part of the spectrum. Table 1 compares the parameters $S_{p,n}$ and $C^m_{p,n}$ derived from the two models. When fitting the two-population model to database A, the assumption is made that as C tends to zero, C_m tends to zero and as a consequence $S_{p,n}C^m_{p,n}$ tends to 1. This assumption is not required for the three-population model as implemented here.

Certain discrepancies can arise when using diagnostic pigments as indicators of phytoplankton size class. For example, the pigment fucoxanthin (the main indicator of diatoms) may also be found in some prymnesiophytes. Therefore, higher percentages of microphytoplankton at low chlorophyll-a concentrations [shown in Fig. 1(e)] may be an artifact of using diagnostic pigments to infer size class. Further investigation into the limitations of using diagnostic pigments to infer cell size is required, possibly by conducting coupled cell count, size-fractionated chlorophyll-a measurements, phytoplankton absorption measurements, and HPLC pigment measurements.

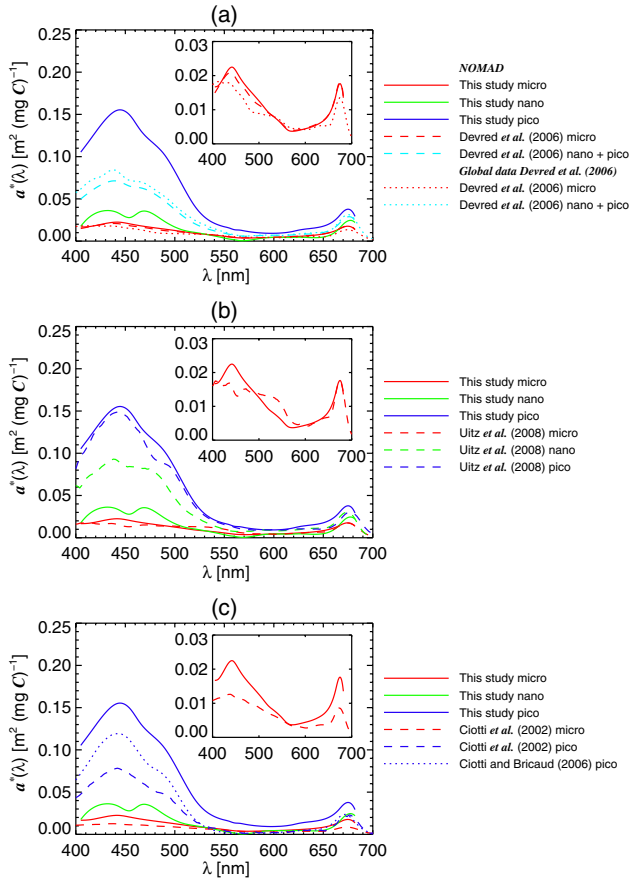

Fig. 6. (Color online) Size-specific $a^*(\lambda)$ coefficients calculated from the three-population model plotted against (a) the two-population model [3], (b) the model of Uitz *et al.* [30], and (c) the model of Ciotti *et al.* [14] (cubic spline used to interpolate between wavelengths in Table 2 for three-population model and the two-population model fitted to database A). For each figure, insets magnify the microplankton spectra.

Figure 4(d) compares the RMSE% of the two models. Over all the 20 wavelengths the three-population model produces lower RMSE%, with a significantly lower average RMSE% between 405 and 550 nm (t-test, $p < 0.05$), indicating a better fit to the data when compared with the two-population model. The values of r (Table 2) are statistically similar across the 20 wavelengths (t-test, $p = 0.77$).

In Fig. 4(a), for chlorophyll-a concentrations less than $0.6\,\mathrm{mg\,m^{-3}}$, the two-population model yields lower $a(\lambda)$ values than both the power-law model and the three-population model. Figure 5(c) shows $a^*(\lambda)$ calculated according to the two-population model, using parameters in Table 2, for a range of chlorophyll-a concentrations. The two-population model constrains its $a^*(\lambda)$ between its $a^*_{p,n}(\lambda)$ and $a^*_m(\lambda)$ values [Fig. 6(a)]. As a consequence, it fails to reproduce the high magnitude of $a^*(\lambda)$ in a picophytoplankton-dominated environment (i.e., at very low chlorophyll-a concentration), seen when superimposing the dominant mean size-class spectra onto Fig. 5(c). Therefore, extending the model from two to three populations (representative of three size classes) improved accuracy and representation of the variability in the specific absorption coefficient at low chlorophyll-a concentration. An advantage of the two-population model is that it can be fitted to any chlorophyll-a and absorption dataset, whereas the three-population model is fitted here using additional information on the size structure of the phytoplankton in the dataset (HPLC data).

2. *Specific Absorption Coefficients of the Three Size Classes of Phytoplankton*

The Model of Uitz et al. [30]

Figure 6(b) compares the specific absorption coefficients calculated using the three-population model with those of Uitz *et al.* [30]. The picophytoplankton coefficients from this study are consistent with those of Uitz *et al.* [30], but the nanophytoplankton coefficients are consistently lower. The two approaches yield similar spectral shapes, with peaks at 490 nm in the picophytoplankton spectra attributable to zeaxanthin and peaks in the nanophytoplankton spectra at around 465 nm, thought to be linked to the presence of 19′-hexanoyloxyfucoxanthin and 19′-butanoyloxyfucoxanthin [48].

The microphytoplankton spectra also differ between the two approaches [Fig. 6(b)]. The $a^*_m(\lambda)$ values are higher in the three-population model in the blue region of the spectrum and lower in the green region compared with Uitz *et al.* [30] and they are similar elsewhere. A majority of data in the Uitz *et al.* [30] study were from the Pacific and Mediterranean Oceans, whereas, the majority of samples in database A were from the Atlantic Ocean. Therefore, diversity in microphytoplankton species would be expected between the two datasets, which could cause variations in $a^*_m(\lambda)$. Furthermore, the data used in Uitz *et al.* [30] varied from 0.02 to $28.7\,\mathrm{mg\,m^{-3}}$ chlorophyll-a (see Table 1 of Uitz *et al.* [30]), whereas the data used in this study varied from 0.04 to $12.2\,\mathrm{mg\,m^{-3}}$ chlorophyll-a, which could also have contributed to the differences.

When applying the Uitz *et al.* [30] model to globally derived chlorophyll-a fields, it is necessary to partition the values into a number of trophic classes before estimating fractions of chlorophyll-a associated with each size class [33]. The mathematical formulation of the three-population model presented here is a continuous function of chlorophyll-a concentration.

The Model of Ciotti et al. [14]

Figure 6(c) shows the specific absorption coefficients calculated using the three-population model and those calculated by Ciotti *et al.* [14]. There are large differences between the two $a^*_p(\lambda)$, with the three-population model giving consistently higher $a^*_p(\lambda)$ values at all wavelengths. In comparison with the data used by Ciotti *et al.* [14], database A incorporates very oligotrophic, tropical waters, such as the North

and South Atlantic gyres. This could explain the higher $a_p^*(\lambda)$ values obtained using the three-population model (see also a similar discussion on the effects of regional representation in Uitz *et al.* [30]).

Figure 6(c) also shows a comparison between $a_p^*(\lambda)$ retrieved using the three-population model and that of Ciotti and Bricaud [43]. The $a_p^*(\lambda)$ spectrum of Ciotti and Bricaud [43] was derived from a *Prochlorococcus* dominated natural population measured in the Equatorial Pacific during the FLUPAC cruise [28], hence, more oligotrophic waters than data used in Ciotti *et al.* [14], which is likely to have resulted in higher $a_p^*(\lambda)$ values at blue wavelengths [Fig. 6(c)]. It is also worth noting that the Ciotti *et al.* [14] $a_p^*(\lambda)$ spectrum was derived under the assumption of a constant β factor [52], without accounting for spectral backscattering losses [53]. Higher $a_p^*(\lambda)$ values are observed in the blue region of the Ciotti and Bricaud [43] absorption spectrum (closer to $a_p^*(\lambda)$ derived using the three-population model) when compared with Ciotti *et al.* [14]. However, despite a better match, $a_p^*(\lambda)$ values derived using the three-population model are consistently higher than those of Ciotti and Bricaud [43], which may have resulted from contrasting methods in deriving $a_p^*(\lambda)$ (e.g., the use of HPLC data or different model formulation).

For the microphytoplankton, $a_m^*(\lambda)$ from the three-population model is slightly higher at all wavelengths compared with that of Ciotti *et al.* [14]. The Ciotti *et al.* [14] database incorporated data with chlorophyll-a concentrations as high as 135 mg m^{-3} (see Table 2 of Ciotti *et al.* [14]). It is possible that, at such large chlorophyll-a concentrations (particularly during an intense bloom of *Gonyaulax digitale* in the Bedford Basin), the sampled microplankton population may well have been different from those encountered at lower concentrations in the open ocean, which could account for the differences in the magnitude of $a_m^*(\lambda)$, also highlighted by Devred *et al.* [3].

C. Remote-Sensing Validation

Remote-sensing reflectances ($R_{rs}(\lambda)$) from database B were used to derive the near-surface chlorophyll-a concentration (C^{sat}) using the Ocean Chlorophyll 4—version 4 (OC4-v4) algorithm [37]. Figure 7(g) shows a comparison between the *in situ* HPLC chlorophyll-a concentrations (C) and the derived C^{sat} concentrations in database B. The two are well correlated ($r = 0.69$) with a RMSE% of 102.5%. Larger differences are associated with samples in more optically complex waters where simple band-ratio algorithms are known to break down [37].

The three-population model [Eq. (20)] was applied to C^{sat} using the parameters in Tables 1 and 2 to derive $a^{sat}(\lambda)$ (total phytoplankton absorption from $R_{rs}(\lambda)$). Comparisons between remotely sensed and *in situ* phytoplankton absorption values at the six SeaWiFS wavelengths are shown in Figs. 7(a)–7(f) and indicate good agreement. The RMSE% varies from 52.5% to 59.2% between the wavelengths of 411–555 nm, increases to 308% at 555 nm due to a very low signal at this wavelength, and is 115.5% in the red region (670 nm). Furthermore, all wavelengths are well correlated ($r > 0.65$). Between 411–555 nm, the three-population model underestimates a^{sat} at high values [e.g., >0.2 m^{-1}, Fig. 7(b)], probably because of differences in the composition of database A compared with database B. Database A, with which the three-population model was parameterized, has chlorophyll-a concentrations ranging from 0.04 to 12.2 mg m^{-3}, with only 10% of the database with chlorophyll-a concentrations greater than 2.0 mg m^{-3}. The corresponding values in database B are from 0.02 to 77.8 mg m^{-3}, with 38% of the database greater than 2.0 mg m^{-3}. Therefore, the parameters in Tables 1 and 2 are not strictly applicable to chlorophyll-a concentrations greater than 12.2 mg m^{-3} and the three-population model appears to underestimate $a^{sat}(443)$ at chlorophyll-a concentrations greater than 2.0 mg m^{-3} when compared with database B [Fig. 7(h)]. Additional HPLC and $a(\lambda)$ data may be required to improve the parameterization of the three-component model at high chlorophyll-a concentrations.

The lowest RMSE% in the validation was for 443 nm [Fig. 7(c)], which may be a result of this wavelength corresponding to the highest value of absorption for a given spectra and, therefore, the lowest signal-to-noise ratio. We computed the absolute RMSE between *in situ* $a(443)$ and $a^{sat}(443)$ for each sample in database B according to

$$\mathrm{RMSE}_i[\mathrm{m}^{-1}] = [(a_{i,E}(\lambda) - a_{i,M}(\lambda))^2]^{1/2}, \qquad (27)$$

where $a(443)$ is the variable (phytoplankton absorption coefficient at 443 nm), i denotes the sample, subscript E denotes the estimated variable ($a^{sat}(443)$), and the subscript M denotes the measured variable ($a(443)$). Figure 7(i) shows the absolute RMSE at 443 nm plotted as a function of $a^{sat}(443)$. Using a log-linear fit, a strong correlation was found between the absolute RMSE at 443 nm and $a^{sat}(443)$ ($r = 0.79$, $p < 0.001$).

Considering that database B includes data from a diversity of locations not present in database A (e.g., Beaufort Sea, Indian Ocean, and Australia-Antarctic Basin) and considering the RMSE% between C^{sat} and the *in situ* chlorophyll-a concentrations in Fig. 7(g) (~102.5%), the RMSE% shown in Figs. 7(a)–7(f) are quite encouraging and support the application of the three-population absorption model to satellite $R_{rs}(\lambda)$ fields. It is envisaged that with improvements in remotely sensed chlorophyll-a retrievals this error would reduce. Furthermore, as shown by Sathyendranath *et al.* [47], through discriminating diatoms from other phytoplankton using ocean-color data, the three-population absorption model may have the potential to improve C^{sat} retrievals from $R_{rs}(\lambda)$.

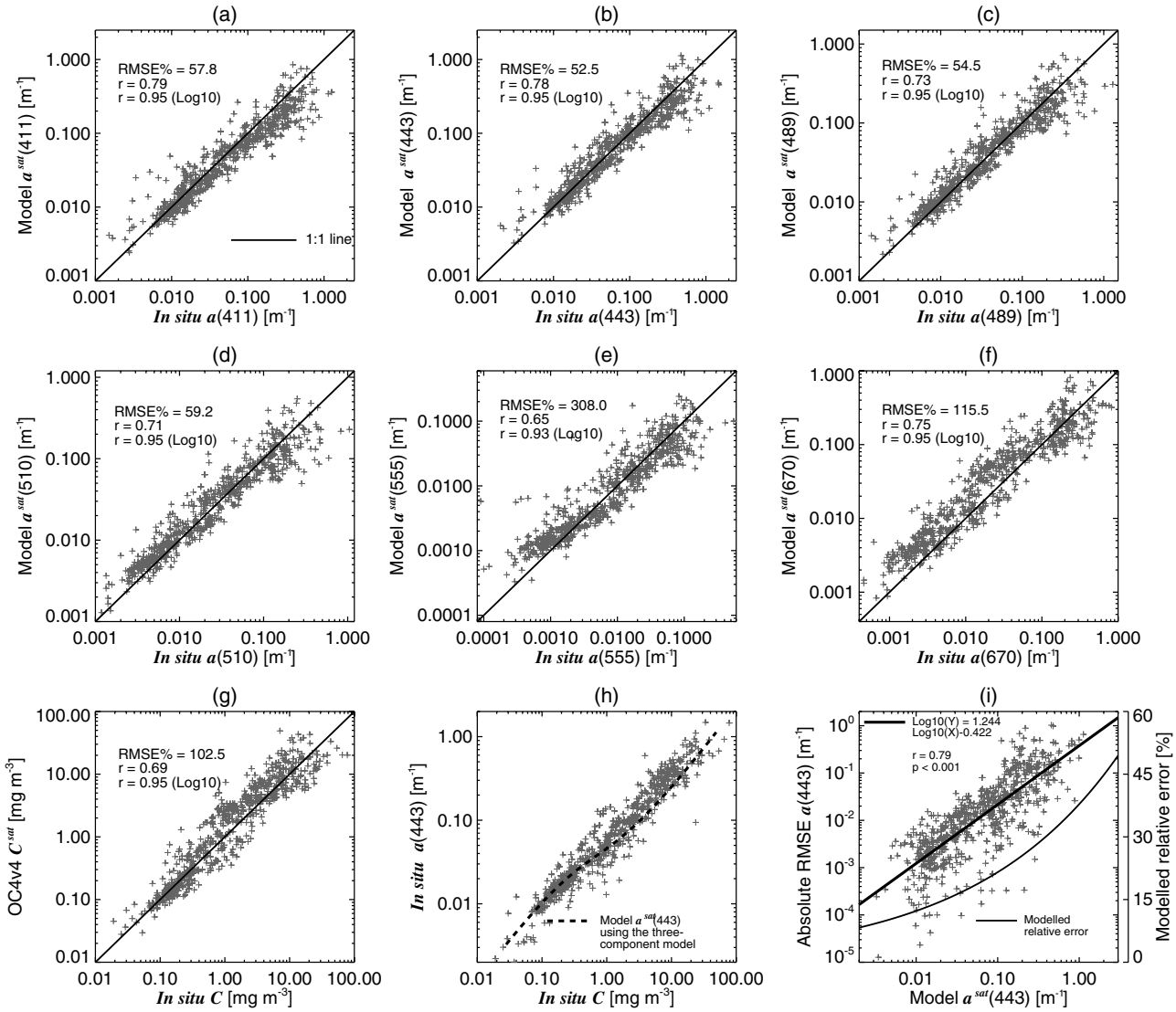

Fig. 7. The $a^{\mathrm{sat}}(\lambda)$ values using the three-population absorption model compared with the *in situ* $a(\lambda)$ values in database B at the wavelengths of (a) 411 nm, (b) 443 nm, (c) 489 nm, (d) 510 nm, (e) 555 nm, and (f) 670 nm, respectively. The relationship between the *in situ* chlorophyll-a concentrations (C) and C^{sat} (OC4v4 [37]) from database B is shown in (g), (h) shows *in situ* $a(443)$ plotted against *in situ* C in database B with $a^{\mathrm{sat}}(443)$ calculated using the three-population model superimposed, and (i) shows the absolute RMSE between $a^{\mathrm{sat}}(443)$ and $a(443)$ plotted as a function of $a^{\mathrm{sat}}(443)$. Linear Pearson correlation coefficients (r) are provided in addition to r values using $\log_{10}$ transformation.

D. Global Application

In light of the results above, we have applied the three-population absorption model to daily, Level 3, SeaWiFS chlorophyll-a composites for May 2005 to produce a monthly composite of total phytoplankton absorption and the absolute and relative estimated error (Fig. 8). Any values greater than 12.2 mg m^{-3} chlorophyll-a were masked. The wavelength of 443 nm was chosen for our example as it was found to have the lowest RMSE% when compared with the *in situ* data [Fig. 7(b)]. We estimated the absolute error according to the log-linear fit described in Fig. 7(i) and estimated the relative error percentage by dividing the absolute error by $a^{\mathrm{sat}}(443)$ and multiplying by 100.

For May 2005, high levels of $a^{\mathrm{sat}}(\lambda)$ are seen in the sub-Arctic, associated with the boreal Spring blooms, in coastal upwelling zones, such as the Benguela, in the southern North Sea, and the area around the Amazon outflow. Lower $a^{\mathrm{sat}}(443)$ values are found in the subtropical oligotrophic gyres. The estimated absolute error is seen to increase with increasing $a^{\mathrm{sat}}(443)$ according to the log-linear fit [Fig. 7(i)]. The estimated relative error is shown to be less than 20% in the majority of the global ocean, increasing to $>40\%$ in the highly eutrophic regions.

Figure 9 shows the estimated absorption coefficient of the three size classes for May 2005. Absorption by microphytoplankton ($a_m^{\mathrm{sat}}(443)$) is high in the sub-Arctic and upwelling zones associated with blooms of diatoms and dinoflagellates; elsewhere, $a_m^{\mathrm{sat}}(443)$ is low. Similar to microphytoplankton, nanophytoplankton absorption ($a_n^{\mathrm{sat}}(443)$) contributes mainly to the eutrophic and mesotrophic

regions. However, when compared with $a_m^{\mathrm{sat}}(443)$, their contribution extends offshore of the coastal upwelling zones and higher $a_n^{\mathrm{sat}}(443)$ values are found in the South and North Atlantic convergence and in equatorial regions.

Picophytoplankton are seen to act as a background population with small variability in $a_p^{\mathrm{sat}}(443)$ globally. This supports the theory first proposed in Yentch and Phinney [44] that a constant background population of small optically active cells are always present, on which larger-celled phytoplankton may be sporadically superimposed. In comparison with microphytoplankton and nanophytoplankton, $a_p^{\mathrm{sat}}(443)$ is higher in the subtropical oligotrophic gyres.

When comparing $a_p^{\mathrm{sat}}(443)$ in Fig. 9 with $a^{\mathrm{sat}}(443)$ in Fig. 8, it can be seen that picoplankton contribute more to $a^{\mathrm{sat}}(443)$ than nanophytoplankton or microphytoplankton. In fact, when the global mean fractional contribution of picophytoplankton to the total phytoplankton absorption in the surface layer for May 2005 is computed using the model $(a_p^{\mathrm{sat}}(443)/a^{\mathrm{sat}}(443) \times 100)$, it emerges that picophytoplankton contribute ~65% to the total phytoplankton absorption coefficient, whereas they contribute only ~23% to the total chlorophyll-a concentration. As picophytoplankton have a higher specific absorption coefficient

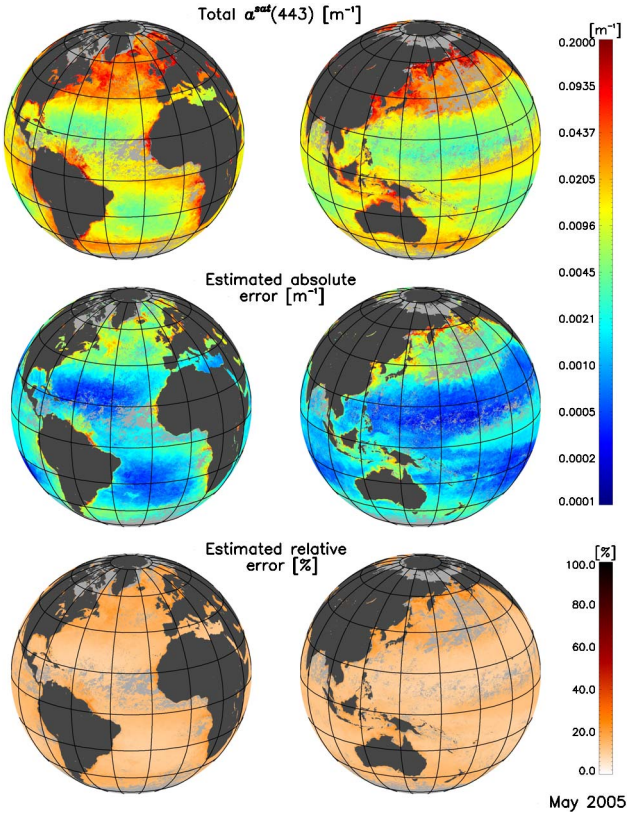

Fig. 8. (Color online) Total $a^{\mathrm{sat}}(443)$ values for May 2005, using SeaWiFS daily composites, calculated according to the three-population absorption model, with the estimated absolute and relative errors. Dark gray pixels represent land, and light gray pixels represent missing data due to cloud coverage, high sun zenith angles, or chlorophyll-a concentrations $>12.2\,\mathrm{mg\,m^{-3}}$.

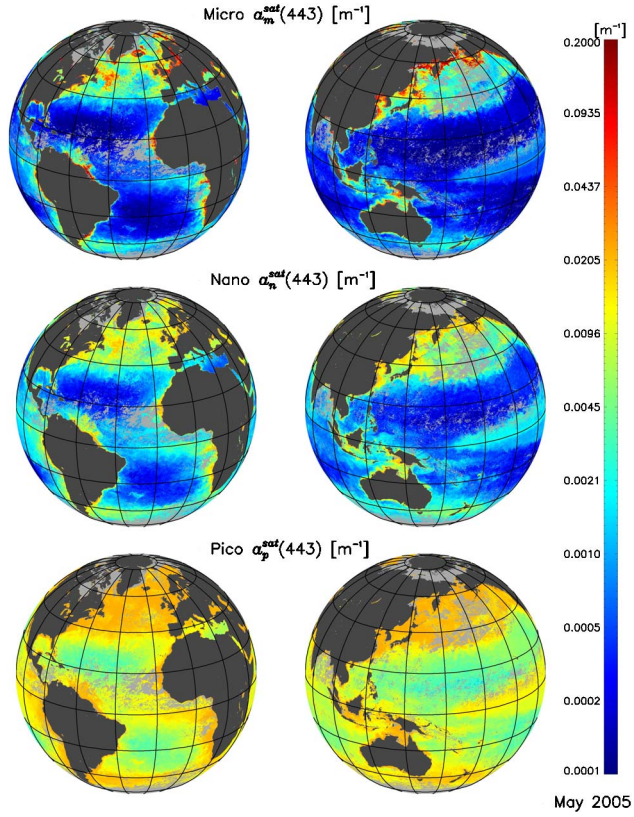

Fig. 9. (Color online) Microphytoplankton, nanophytoplankton, and picophytoplankton absorption coefficients at 443 nm for May 2005, using SeaWiFS daily composites, calculated according to the three-population absorption model. Dark gray pixels represent land, and light gray pixels represent missing data due to cloud coverage, high sun zenith angles, or chlorophyll-a concentrations $>12.2\,\mathrm{mg\,m^{-3}}$.

than nanophytoplankton or microphytoplankton (Fig. 2), they are more efficient in absorbing light and, hence, have a larger influence on $a^{\mathrm{sat}}(443)$ globally than may be inferred from their chlorophyll-a concentration alone. Considering $a(\lambda)$ is an important property in primary production models, the three-population model can be used to improve primary production estimates by explicitly accounting for size structure [16,54,55].

Figures 8 and 9 show estimates of total and size-specific phytoplankton absorption based on the three-population model fitted to globally representative data (database A). However, we acknowledge that a global parameterization may not fully capture the wide-scale variability in phytoplankton physiology. Devred *et al.* [3] highlighted regional and seasonal variability in the parameters of their two-component model. Future work may need to focus on such temporal and spatial differences, possibly partitioning data into biogeochemical provinces and dealing with each province independently [56,57].

4. Summary

A model has been developed that calculates the phytoplankton absorption coefficient at various wavelengths based on three-component populations of

phytoplankton which, with some caution, can be linked to the three size classes of phytoplankton (picophytoplankton, nanophytoplankton, and microphytoplankton). When compared with the two-population model, the new model yielded lower errors. Furthermore, the three-population model is an improvement on traditional power-law models in that the parameters of the model offer direct biological and bio-optical interpretation, and that the specific absorption coefficients are constrained between limits set by the values of those of picophytoplankton and microphytoplankton [2,3]. At the same time, the three-population absorption model extends the model of Sathyendranath *et al.* [2] and Devred *et al.* [3] by introducing a third component population. This implementation yields a better representation of both $a^*(\lambda)$ and $a(\lambda)$ at low chlorophyll-a concentrations.

The computed size-specific $a^*(\lambda)$ values were compared with those derived by Ciotti *et al.* [14] and Uitz *et al.* [30]. Unlike the model of Ciotti *et al.* [14], the three-population model can be used to predict how $a^*(\lambda)$ would change with varying pigment concentrations. Unlike the model of Uitz *et al.* [30], when applying the three-population model to globally derived chlorophyll-a fields, the model can be applied to a continuum of chlorophyll-a concentrations without having to rely on a small number of class intervals indicative of trophic regimes. The computed size-specific $a^*(\lambda)$ values compare reasonably well with laboratory and *in situ* measurements.

The three-population model was applied to remotely sensed chlorophyll-a data and validated using independent *in situ* data, which indicated good agreement. It is expected this accuracy will improve with advancements in remotely sensed chlorophyll-a retrievals. It is envisaged that the three-population model can be used to improve primary production estimates by explicitly incorporating community composition [16,54,55].

Appendix A

Definitions of the symbols used in this manuscript are provided in the table.

Symbol	Definition
$a(\lambda)$	Absorption coefficient of total phytoplankton [m^{-1}]
$a_m(\lambda)$	Absorption coefficient of microphytoplankton [m^{-1}]
$a_n(\lambda)$	Absorption coefficient of nanophytoplankton [m^{-1}]
$a_p(\lambda)$	Absorption coefficient of picophytoplankton [m^{-1}]
$a^{sat}(\lambda)$	Absorption coefficient of total phytoplankton derived from R_{rs} [m^{-1}]
$a_m^{sat}(\lambda)$	Absorption coefficient of microphytoplankton derived from R_{rs} [m^{-1}]
$a_n^{sat}(\lambda)$	Absorption coefficient of nanophytoplankton derived from R_{rs} [m^{-1}]
$a_p^{sat}(\lambda)$	Absorption coefficient of picophytoplankton derived from R_{rs} [m^{-1}]
$a^*(\lambda)$	Specific absorption coefficient of total phytoplankton (m^2 [mg C]$^{-1}$)
$a_m^*(\lambda)$	Specific absorption coefficient of microphytoplankton (m^2[mg C]$^{-1}$)
$a_n^*(\lambda)$	Specific absorption coefficient of nanophytoplankton (m^2 [mg C]$^{-1}$)
$a_p^*(\lambda)$	Specific absorption coefficient of picophytoplankton (m^2 [mg C]$^{-1}$)
$a_{p,n}^*(\lambda)$	Specific absorption coefficient of combined pico-nanophytoplankton (m^2 [mg C]$^{-1}$)
A	Numerical constant derived using the power-law model [Eq. (22)]
B	Numerical constant derived using the power-law model [Eq. (22)]
C	Total chlorophyll-a concentration derived from high performance liquid chromatography [mg m^{-3}]
C^{sat}	Total chlorophyll-a concentration derived from $R_{rs}(\lambda)$ following O'Reilly *et al.* [37] [mg m^{-3}]
C_m	Chlorophyll-a concentration of microphytoplankton [mg m^{-3}]
C_n	Chlorophyll-a concentration of nanophytoplankton [mg m^{-3}]
C_p	Chlorophyll-a concentration of picophytoplankton [mg m^{-3}]
$C_{p,n}$	Chlorophyll-a concentration of combined pico-nanophytoplankton [mg m^{-3}]
C_w	Total chlorophyll-a concentration [mg m^{-3}] derived from P and W according to Uitz *et al.* [33]
$C_{p,n}^m$	Maximum chlorophyll-a concentration of combined pico-nanophytoplankton [mg m^{-3}]
C_p^m	Maximum chlorophyll-a concentration of picophytoplankton [mg m^{-3}]
F_m	Microphytoplankton fraction of chlorophyll-a
F_n	Nanophytoplankton fraction of chlorophyll-a
F_p	Picophytoplankton fraction of chlorophyll-a
$F_{p,n}$	Combined pico-nanophytoplankton fraction of chlorophyll-a
P	Diagnostic pigments (fucoxanthin; peridinin; 19′-hexanoyloxyfucoxanthin; 19′-butanoyloxyfucoxanthin; alloxanthin; chlorophyll-b and divinyl chlorophyll-b; zeaxanthin)
r	Pearson correlation coefficient
R	Size-specific slopes describing the variations in the size-specific $a^*(\lambda)$ of the Uitz *et al.* [30] model along the vertical z/Z_p
RMSE %	Relative root mean square error [%] [Eq. (21)]
RMSE	Absolute root mean square error [m^{-1}] [Eq. (27)]
R_{rs}	Remote-sensing reflectance [sr^{-1}]
$S_{p,n}$	Slope describing the rate of increase in the chlorophyll-a concentration of combined pico-nanophytoplankton as a function of the total chlorophyll-a concentration
S_p	Slope describing the rate of increase in the chlorophyll-a concentration of picophytoplankton as a function of the total chlorophyll-a concentration
W	Chlorophyll-a to diagnostic pigment ratios derived by Uitz *et al.* [33] (1.41; 1.41; 1.27; 0.35; 0.6; 1.01; 0.86)
z	Geometric depth [m]
Z_p	Euphotic depth [m]

The authors thank both SeaBASS and all contributors to the NOMAD dataset for *in situ* data. SeaWiFS data used in this publication were produced by the SeaWiFS project at the Goddard Space Flight Center. The data were obtained from the Goddard Earth Sciences Distributed Active Archive Center under the auspices of the National Aeronautics and Space Administration (NASA). Use of this data

is in accord with the SeaWiFS Research Data Use Terms and Agreements. This work is funded by the National Environmental Research Council (NERC), UK, through a Ph.D. studentship, the National Centre for Earth Observation and NERC Oceans 2025 programme (Themes 6 and 10). We thank Aurea Ciotti and Annick Bricaud for providing specific absorption coefficients for a *Prochlorococcus* dominated natural population measured in the Equatorial Pacific during the FLUPAC cruise. We also thank the reviewers and the editor for helpful comments on the previous version of the manuscript. This is a contribution to the Ocean Colour Climate Change Initiative of the European Space Agency.

References

1. R. J. W. Brewin, S. Sathyendranath, T. Hirata, S. Lavender, R. M. Barciela, and N. J. Hardman-Mountford, "A three-component model of phytoplankton size class for the Atlantic Ocean," Ecol. Modelling **221**, 1472–1483 (2010).
2. S. Sathyendranath, V. Stuart, G. Cota, H. Mass, and T. Platt, "A two-component model of phytoplankton absorption in the open ocean: theory and applications," Int. J. Remote Sens. **22**, 249–273 (2001).
3. E. Devred, S. Sathyendranath, V. Stuart, H. Mass, O. Ulloa, and T. Platt, "Remote sensing of phytoplankton pigments: a comparison of empirical and theoretical approaches," J. Geophys. Res. **111**, C03011 (2006).
4. J. T. O. Kirk, "A theoretical analysis of the contribution of algal cells to the attenuation of light within waters. I. General treatment of suspensions of living cells," New Phytol. **75**, 1–20 (1975).
5. A. Morel, "Available, usable, and stored radiant energy in relation to marine photosynthesis," Deep-Sea Res. **25**, 673–688 (1978).
6. A. Morel, "Optical modeling of the upper ocean in relation to its biogenous matter content (Case I waters)," J. Geophys. Res. **93**, 10749–10768 (1988).
7. S. Sathyendranath and T. Platt, "The spectral irradiance field at the surface and in the interior of the ocean: a model for applications in oceanography and remote sensing," J. Geophys. Res. **93**, 9270–9280 (1988).
8. T. Anderson, "A spectrally averaged model of light penetration and photosynthesis," Limnol. Oceanogr. **38**, 1403–1419 (1993).
9. T. Platt and A. D. Jassby, "The relationship between photosynthesis and light for natural assemblages of coastal marine-phytoplankton," J. Phycol. **12**, 421–430 (1976).
10. D. A. Kiefer and B. G. Mitchell, "A simple steady state description of phytoplankton growth based on absorption cross section and quantum efficiency," Limnol. Oceanogr. **28**, 770–776 (1983).
11. T. Platt and S. Sathyendranath, "Oceanic primary production: estimation by remote sensing at local and regional scales," Science **241**, 1613–1620 (1988).
12. T. J. Smyth, G. F. Moore, T. Hirata, and J. Aiken, "Semianalytical model for the derivation of ocean color inherent optical properties: description, implementation, and performance assessment," Appl. Opt. **45**, 8116–8131 (2006).
13. J. Marra, C. Trees, and J. O'Reilly, "Phytoplankton pigment absorption: a strong predictor of primary productivity in the surface ocean," Deep-Sea Res., Part I **54**, 155–163 (2007).
14. A. M. Ciotti, M. R. Lewis, and J. J. Cullen, "Assessment of the relationships between dominant cell size in natural phytoplankton communities and the spectral shape of the absorption coefficient," Limnol. Oceanogr. **47**, 404–417 (2002).
15. T. Hirata, J. Aiken, N. J. Hardman-Mountford, and T. J. Smyth, "An absorption model to derive phytoplankton size classes from satellite ocean colour," Remote Sens. Environ. **112**, 3153–3159 (2008).
16. T. Hirata, N. J. Hardman-Mountford, R. Barlow, T. Lamont, R. J. W. Brewin, T. J. Smyth, and J. Aiken, "An inherent optical property approach to the estimation of size-specific photosynthetic rates in eastern boundary upwelling zones from satellite ocean colour: an initial assessment," Prog. Oceanogr. **83**, 393–397 (2009).
17. L. Prieur and S. Sathyendranath, "An optical classification of coastal and oceanic waters based on the specific spectral absorption curves of phytoplankton pigments, dissolved organic matter and other particulate materials," Limnol. Oceanogr. **26**, 671–689 (1981).
18. J. S. Cleveland, "Regional models for phytoplankton absorption as a function of chlorophyll a concentration," J. Geophys. Res. **100**, 13333–13344 (1995).
19. V. A. Lutz, S. Sathyendranath, and E. J. H. Head, "Absorption coefficient of phytoplankton: regional variations in the North Atlantic," Mar. Ecol. Prog. Ser. **135**, 197–213 (1996).
20. A. Bricaud, H. Claustre, J. Ras, and K. Oubelkheir, "Natural variability of phytoplanktonic absorption in oceanic waters: influence of the size structure of algal populations," J. Geophys. Res. **109**, C11010 (2004).
21. J. T. O. Kirk, "A theoretical analysis of the contribution of algal cells to the attenuation of light within waters. II. Spherical cells," New Phytol. **75**, 21–36 (1975).
22. A. Morel and A. Bricaud, "Theoretical results concerning light absorption in a discrete medium, and application to specific absorption of phytoplankton," Deep-Sea Res. **28**, 1375–1393 (1981).
23. S. Sathyendranath, S. L. Lazzara, and L. Prieur, "Variations in the spectral values of specific absorption of phytoplankton," Limnol. Oceanogr. **32**, 403–415 (1987).
24. N. Hoepffner and S. Sathyendranath, "Effect of pigment composition on absorption properties of phytoplankton," Mar. Ecol. Prog. Ser. **73**, 11–23 (1991).
25. S. E. Lohrenz, A. D. Weidemann, and M. Tuel, "Phytoplankton spectral absorption as influenced by community size structure and pigment composition," J. Plankton Res. **25**, 35–l61 (2003).
26. A. Morel, "Light and marine photosynthesis: A spectral model with geochemical and climatological implications," Prog. Oceanogr. **26**, 263–306 (1991).
27. A. Bricaud, M. Babin, A. Morel, and H. Claustre, "Variability in the chlorophyll-specific absorption coefficients of natural phytoplankton: analysis and parameterization," J. Geophys. Res. **100**, 13321–13332 (1995).
28. A. Bricaud, A. Morel, M. Babin, K. Allali, and H. Claustre, "Variations of light absorption by suspended particles with the chlorophyll a concentration in oceanic (case 1) waters: analysis and implications for bio-optical models," J. Geophys. Res. **103**, 31033–31044 (1998).
29. L. N. M. Duysens, "The flattening of the absorption spectrum of suspensions as compared to that of solutions," Biochim. Biophys. Acta **19**, 1–12 (1956).
30. J. Uitz, Y. Huot, F. Bruyant, M. Babin, and H. Claustre, "Relating phytoplankton photophysiological properties to community structure on large scales," Limnol. Oceanogr. **53**, 614–630 (2008).
31. A. M. Waite and P. S. Hill, "Flocculation and phytoplankton cell size can alter ^{234}Th-based estimates of the vertical flux of particulate organic carbon in the sea," Mar. Chem. **100**, 366–375 (2006).
32. F. Vidussi, H. Claustre, B. B. Manca, A. Luchetta, and J. C. Marty, "Phytoplankton pigment distribution in relation to upper thermocline circulation in the eastern Mediterranean Sea during winter," J. Geophys. Res. **106**, 19939–19956 (2001).

33. J. Uitz, H. Claustre, A. Morel, and S. B. Hooker, "Vertical distribution of phytoplankton communities in open ocean: an assessment based on surface chlorophyll," J. Geophys. Res. **111**, CO8005 (2006).
34. H. Claustre, M. Babin, D. Merien, J. Ras, L. Prieur, S. Dallot, O. Prasil, and H. Dousova, "Towards a taxon-specific parameterization of bio-optical models of primary production: a case study in the North Atlantic," J. Geophys. Res. **110**, C07S12 (2005).
35. P. J. Werdell and S. W. Bailey, "An improved in situ bio-optical data set for ocean colour algorithm development and satellite data production validation," Remote Sens. Environ. **98**, 122–140 (2005).
36. J. Aiken, Y. Pradhan, R. Barlow, S. Lavender, A. Poulton, P. Holligan, and N. J. Hardman-Mountford, "Phytoplankton pigments and functional types in the Atlantic Ocean: a decadal assessment, 1995–2005. AMT Special Issue," Deep-Sea Res., Part II **56**, 899–917 (2009).
37. J. E. O'Reilly, S. Maritorena, B. G. Mitchell, D. A. Siegel, K. L. Carder, S. A. Garver, M. Kahru, and C. McClain, "Ocean chlorophyll algorithms for SeaWiFS," J. Geophys. Res. **103**, 24937–24953 (1998).
38. J. Werdell, "Global bio-optical algorithms for ocean color satellite applications," EOS Trans. AGU **90**, 4 (2009).
39. W. H. Press, S. A. Keukolsky, W. T. Vettering, and B. P. Flannery, *Levenberg-Marquard Method in Numerical Recipes in C: the Art of Scientific Computation* (Cambridge Univeristy, 1992).
40. F. Partensky, N. Hoepffner, W. K. W. Li, O. Ulloa, and D. Vaulot, "Photoacclimation of *Prochlorococcus sp* (Prochlorophyta) strains isolated from the North Atlantic and the Mediterranean Sea," Plant Physiol. **101**, 285–296 (1993).
41. Z. V. Finkel, "Light absorption and size scaling of light-limited metabolism in marine diatoms," Limnol. Oceanogr. **46**, 86–94 (2001).
42. M. Babin, A. Morel, H. Claustre, and A. Bricaud, "Nitrogen- and irradiance- dependant variations of the maximum quantum yield of carbon fixation in eutrophic, mesotrophic and oligotrophic marine systems," Deep-Sea Res., Part I **43**, 1241–1272 (1996).
43. A. M. Ciotti and A. Bricaud, "Retrievals of a size parameter for phytoplankton and spectral light absorption by colored detrital matter from water-leaving radiances at SeaWiFS channels in a continental shelf region off Brazil," Limnol. Oceanogr. Methods **4**, 237–253 (2006).
44. C. S. Yentsch and D. A. Phinney, "A bridge between ocean optics and microbial ecology," Limnol. Oceanogr. **34**, 1694–1704 (1989).
45. V. Stuart, S. Sathyendranath, T. Platt, H. Mass, and B. Irwin, "Pigments and species composition of natural phytoplankton populations: effects on the absorption spectra," J. Plankton Res. **20**, 187–217 (1998).
46. V. Stuart, S. Sathyendranath, E. J. H. Head, T. Platt, B. Irwin, and H. Mass, "Bio-optical characteristics of diatom and prymnesiophyte populations in the Labrador Sea," Mar. Ecol. Prog. Ser. **201**, 91–106 (2000).
47. S. Sathyendranath, L. Watts, E. Devred, T. Platt, C. Caverhill, and H. Mass, "Discrimination of diatoms from other phytoplankton using ocean-colour data," Mar. Ecol. Prog. Ser. **272**, 59–68 (2004).
48. S. W. Jeffrey and R. F. C. Mantoura, "Development of pigment methods for oceanography: SCOR-supported working groups and objectives," in *Phytoplankton Pigments in Oceanography: Guidelines to Modern Methods*, S. W. Jeffrey, R. F. C. Mantoura, and S. W. Wright, eds. (UNESCO Publishing, 1997), pp 38–84.
49. R. Barlow, J. Aiken, P. Holligan, D. G. Cummings, S. Maritorena, and S. B. Hooker, "Phytoplankton pigment and absorption characteristics along meridional transects in the Atlantic Ocean," Deep-Sea Res., Part I **49**, 637–660 (2002).
50. A. Morel, Y. H. Ahn, F. Partensky, D. Vaulot, and H. Claustre, "*Prochlorococcus* and *Synechococcus*: a comparative study of their optical properties in relation to their size and pigmentation," J. Mar. Res. **51**, 617–649 (1993).
51. L. R. Moore, R. Goericke, and S. W. Chisholm, "Comparative physiology of *Synechococcus* and *Prochlorococcus*: influence of light and temperature on growth, pigments, fluorescence and absorptive properties," Mar. Ecol. Prog. Ser. **116**, 259–275 (1995).
52. C. S. Roesler, "Theoretical and experimental approaches to improve the accuracy of particulate absorption coefficients derived from the quantitative filter technique," Limnol. Oceanogr. **43**, 1649–1660 (1998).
53. A. M. Ciotti, A. Bricaud, and S. A. Gaeta, "Retrieval of a size parameter for phytoplankton from spectral water-leaving radiances in the SeaWiFS channels," presented at Ocean Optics XVII, Freemantle, Australia, 25–29 October 2004.
54. J. Uitz, H. Claustre, F. Brian Griffiths, J. Ras, N. Garcia, and V. Sandroni, "A phytoplankton class-specific primary production model applied to the Kerguelen Islands region (Southern Ocean)," Deep-Sea Res., Part. I **56**, 541–560 (2009).
55. J. Uitz, H. Claustre, B. Gentili, and D. Stramski, "Phytoplankton class-specific primary production in the world's oceans: seasonal and interannual variability from satellite observations," Global Biogeochem. Cycles **24**, GB3016 (2010).
56. N. J. Hardman-Mountford, T. Hirata, K. A. Richardson, and J. Aiken, "An objective methodology for the classification of ecological pattern into biomes and provinces for the pelagic ocean," Remote Sens. Environ. **112**, 3341–3352 (2008).
57. E. Devred, S. Sathyendranath, and T. Platt, "Decadal changes in ecological provinces of the Northwest Atlantic Ocean revealed by satellite observations," Geophys. Res. Lett. **36**, L19607 (2009).